INTERNATIONAL JOURNAL OF CONSERVATION SCIENCE
ISSN: 2067-533X Volume 15, Issue 3, 2024: 1259-1286 www.ijcs.ro
DOI: 10.36868/IJCS.2024.03.08

EXTENDED MONITORING AS SUPPORT IN NUMERICAL MODELLING OF COMPLEX HISTORICAL TIMBER STRUCTURE

Zdzisław Mikołaj PAWLAK[1*], Piotr MARCINIAK[2], Ireneusz WYCZAŁEK[3], Martyna ŻAK-SAWIAK[1]

[1] Institute of Structural Analysis, Poznan University of Technology, 60-965 Poznań, Poland
[2] Institute of Architecture, Urban Planning and Heritage Protection, Poznan University of Technology, 60-965 Poznań, Poland
[3] Faculty of Civil and Environmental Engineering and Architecture, Bydgoszcz University of Science and Technology, 85-796 Bydgoszcz, Poland

Abstract

To support the conservation efforts regarding a wooden church in Domachowo, extensive research and design work was required to strengthen its weakened structure. A variety of data and analyses are necessary to make an accurate assessment, including obtaining a computational model, monitoring the behavior of the structure and its response to external forces and also performing strength analyses and verifying them with measurement data. For accurate geometric evaluation, static and dynamic measurements were required. A mathematical model and a flowchart of the necessary tasks were developed, along with the selection and installation of measuring devices. For this particular structure, static measurements were made using an automatic total station and dynamic measurements using tilt sensors. The purpose of the analysis was to correlate the inertia measurements with the absolute tachymetric observations related to reference points fixed outside the object in order to accurately assess the behavior of the object. Another important issue was to model the column element under study in such a way that its horizontal displacements could be determined from the measured inclinations. The obtained results indicated the need to strengthen the joints of the two main parts of the structure in order to minimize the impact of dynamic weather conditions. The paper describes the measurement process, the method of calculating displacements and the correlation of both types of data. Selected results confirming the conclusions are also presented.

Keywords*: Historic wooden structure; Continuous monitoring; Inclination measurements; Numerical model; Static and dynamic analysis*

Introduction

Wood is a very popular building material and has been widely used for millennia due to its availability, easy processing and low weight, which is especially important in transport. The disadvantages of wooden structures include sensitivity to changing weather conditions and low resistance to fire, biological pests and biological corrosion. For these reasons, preserved historic wooden structures require special care, both in terms of protecting them from degradation and destruction, as well as ensuring proper load-bearing capacity and structural stability.

The literature offers numerous examples of historic buildings with wooden structural elements [1-4]. Usually, before undertaking any conservation or repair work, it is necessary to conduct a diagnosis of the technical condition of such constructions. Some texts [5-7] describe

* Corresponding author: zdzislaw.pawlak@put.poznan.pl

the diagnostic stages and guidelines for evaluating historic structures, which were developed on the basis of practical research.

A crucial factor in evaluating the condition of a building is determining the mechanical parameters of the built-in wood. *A. Cavalli et al.* [8] reviews the mechanical parameters of wood with a focus on factors that affect changes of these properties over time, which especially applies to wood in historic buildings. The parameters can be determined using both destructive and non-destructive methods, the latter being extremely useful in tests performed directly in historic buildings. Semi-destructive methods for testing the mechanical parameters of wood have been reviewed by *M. Kloiber et al.* [9]. Among these methods are those that involve taking small samples of wood from the existing structures, those in which a pin is pressed in, a nail is driven in or predrilled screw is pulled out and those in which resistance to drilling a hole is tested. Methods that do not destroy structural elements, but disturb them to some extent, can be used in historic buildings, but non-destructive methods [10], which are not invasive at all, are more suitable in this case. Non-destructive methods include organoleptic testing, as well as acoustic and radiological methods. *F. Arriaga et al.* [11] describes the non-destructive acoustic method for testing wooden elements, although the tests were conducted in a laboratory on an element cut from an existing structure. Paper [12] reviews of acoustic methods for, among other things, monitoring and damage detection in wooden elements. While in [13] the effect of moisture content on the mechanical parameters of wooden structures is analyzed, where the tests were conducted using non-destructive and semi-destructive methods.

In most cases, the mechanical parameters of the built-in materials are determined only once, since their changes are slow. In case of any ambiguity, the evaluation of the technical condition of the wooden structure can be repeated periodically. Similarly, measurements of any deformation in the structure can also be repeated periodically and even monitored continuously. In general, however, the monitoring of historic buildings is limited to periodic inspections and measurements of deformations [14]. Nevertheless, advanced methods of measuring deformation in wooden structures are now available that also allow continuous recording of readings. Such methods are widely used, for example, to monitor bridges [15, 16], although in recent years there has been an increase in the application of these methods to measure displacements in operating buildings [17].

Regarding existing buildings, instead of continuous measurements of deformation, it seems more important to accurately represent their structure in a numerical model in order to assess the level of stresses. In the case of existing wooden structures, numerical modelling techniques can be used to assess both their safety and their resistance to seismic loads [18]. Numerical modelling and the finite element method (FEM) facilitate detailed analyses of the operation of a structure or its individual parts, as well as the analysis of interactions between individual parts made of different materials [19].

The development of a new technology, building information modeling (BIM), based on the creation of an intelligent, virtual model, has revolutionized the approach to building design and management. The model includes a numerical representation of all technical and functional properties of the building and its components, including costs and property rights. In the case of new buildings, the data can be used throughout their entire lifecycle of the object: from early concept development, then during construction, operation and management, until demolition. BIM can also be used for reconstruct or extened existing buildings, as well as for documenting cultural heritage and managing historic buildings [20-23].

This article describes the results of several years of observation of a historic church building with a complex wooden structure. The results of numerical analyses of the computational model built on the basis of the observation are also presented. The main goals of the study were to assess the condition of the existing building, identify its weaknesses and control its response to climatic loads. The first part of the paper describes the structure of the building, which consists of several units built at different times. In the following section, the

methodology of testing and the results of measurements made in an actual structure subjected to various atmospheric influences are presented. The next part shows the results of dynamic analyses based on vibration measurements during high winds. The subsequent part describes the numerical model of the spatial bar structure, based on which static and dynamic analyses were performed, including comparative and parametric analyses. The paper ends with a summary and final conclusions.

Description of the building

The object of the study is the church of St. Michael the Archangel in Domachowo, Poland. Until recently, it was believed to have been built in 1568, but fragments of log walls with paintings dating back to the 14th century have recently been discovered inside. The central section of the building is a single-nave body with a narrower, elongated chancel ending in a three-bay wall (Fig. 1). A chapel adjoins the chancel to the south and a sacristy to the north. A side aisle adjoins the south side of the originally built nave. On the west side, there is a vestibule and a square tower with a porch on the ground floor and two annexes on both sides.

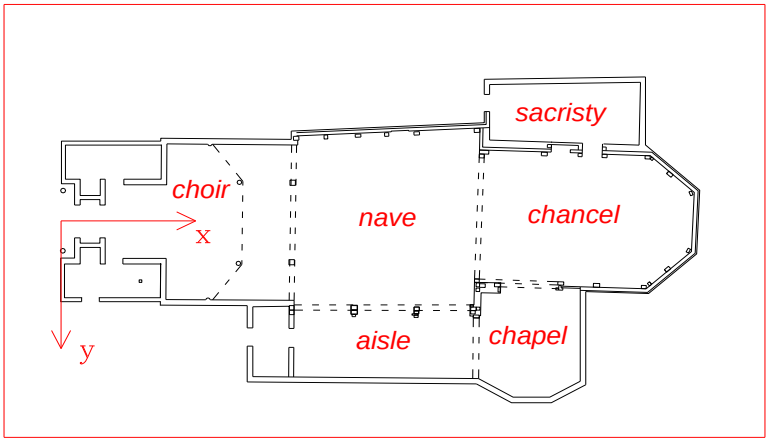

Fig. 1. Ground plan of the building with the division into different sections

The chancel and the nave have separate roofs. The considerably lower sacristy is covered with a single-pitched roof, while the chapel with a gabled roof. The roof system consists of two separate king-post trusses made of oak wood. Their characteristic feature is the central bracing frames, which form poles called king posts.

The church building has a double wall structure. The original log walls were made of oak beams with a cross section of about 13x50 cm. Later, the walls were reinforced with an internal post and beam structure made of pine wood.

Many studies mention the subsequent construction stages. According to existing historiography, the brick sacristy was added in 1586. A major renovation which included adding a new sacristy, rebuilding the tower and reinforcing the walls with an internal timber frame, took place in 1775. The numerous reconstructions and extensions were related, among other things, to the fires that occurred in the 17th and 18th centuries. The building acquired its present form in the 1920s, when a side aisle was added to the south and a wooden frame structure to the west. Furthermore, the tower was replaced and a wooden chapel was erected next to the chancel. Currently, the main load-bearing system is a post and beam frame connected to oak log walls, which are well preserved in the oldest section of the building, the chancel and nave. The successive construction stages of the church's construction are evident in

its spatial structure, namely in the way the wooden elements are arranged, the way the particular parts are connected and the type of material used [20].

Since 2017, the church in Domachowo has been subject to conservation work, which includes the preservation of the polychrome ceiling in the chancel and the nave, as well as wooden furnishings. In 2018, the researchers discovered a gothic rood beam, as well as figural and ornamental polychromes on the logs and on elements of the post and beam, dating probably from the 16th century.

In 2019, the wood was sampled for dendrochronological analyses, which revealed that the wood for the construction of the church was felled in 1368 and 1369. Accordingly, Jerzy Borwiński, a conservator and expert on historic buildings, specifies 1369 as the construction date of the church in Domachowo. This would mean that this is the oldest, almost completely preserved wooden church in Poland.

Description of the structure

Structural assumptions for different sections of the building

The wooden structure of the church is a complex spatial system consisting of several sections that differ in shape, time of construction and carpentry techniques. The main ridge of the roof and the central axis of the building are oriented in a west-east direction (Fig. 2). The main entrance and the porch are situated on the west side. This is followed by the choir and the nave terminating in the chancel.

The oldest section is the chancel. It was built on a rectangular plan measuring about 7.0 x 11.0 meters with two beveled corners on the eastern side (Fig. 1). Originally, the main load-bearing element of this section was the log walls on which the roof trusses rested. Over time, the log beams became deformed, which is probably why the chancel walls on the inside were braced with a frame of posts and beams. Above the walls, there is a king post truss, which carries the weight of the roofing and supports the boarding of the ceiling and the attic floor. The king post truss is approximately 10.0m high, which, with a span of 7.0m results in a roof slope angle of about 69 degrees (264%).

The nave is 9.5m long, counting in the axes of the outermost columns. And its span varies from 9.4 to 9.8m, which indicates that the side walls are not parallel to each other (Fig. 1). As in the chancel, the side walls are of two types of construction: log on the outside and post-and-beam on the inside. The chancel adjoins the nave without any partition, whilst the difference in the width of the two sections is made up for by two short log side walls.

a) b)

Fig. 2. View of the church: a) from the southwest, b) from the northeast

Between these walls, in the middle, there is a rood beam with a span of about 7.7m, which is supported by an additional post and beam system with angle braces (Fig. 3). A ceiling girder, which runs along the nave, rests with one end on the rood beam, in the middle of its span. The second support of the girder is a three-span beam located in the plane where the nave meets the newer, western section of the building. The three-span beam, in turn, rests on the two inner posts and at the ends on the outer walls (Fig. 4).

The girder, along with the entire ceiling plane, is lowering towards the west by more than 20cm. A 10.0m high king post truss rests on the side walls, but due to the longer span of the nave in relation to the chancel (Figs. 1 and 5), the inclination angle of the roof slope is slightly different, being about 64 degrees (205%).

Fig. 3. View of the rood beam from the nave side

Fig. 4. View of the three-span beam supporting the nave girder from the choir section

In general, the entire body of the nave tilts to the west, the entire wall panels, beams and columns, as well as the ceiling in whole are turned. The largest displacements are in the chancel, which leans evenly toward the west within a range of about 16 to 21cm. In the

transverse direction, the pillars of the north and south walls have been displaced and these walls lean towards the interior of the church. The deformation probably occurred due to degradation and lowering of the supports on the west side. Since the floor has been levelled and is now horizontal, the walls of the nave at the west end are lower by about 20 cm compared to the east end.

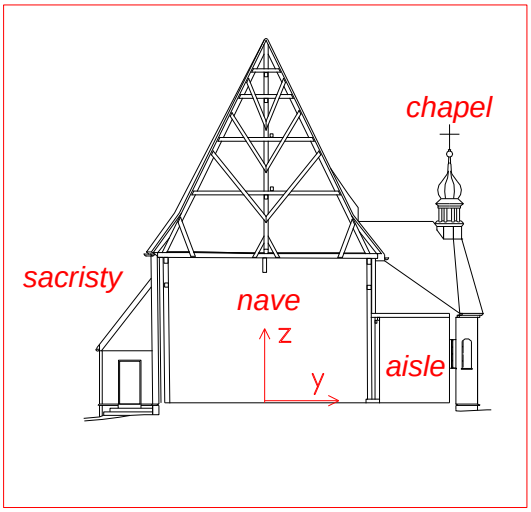

Fig. 5. Cross-section of the nave

The newer section, that is the entrance with the porch and choir, consists of regular cuboid structures with even and mutually perpendicular walls. Above the porch is a tower based on a square plan with a post-and-beam frame, topped by a hipped roof. In the choir section is a mezzanine, the ceiling of which rests on three perimeter walls, while on the nave sides the mezzanine ceiling rests on edge beams supported by two columns (Fig. 4). This section is also topped by a gable roof, whose ridge is a continuation of the ridge of the nave, but this roof is lower, its height is about 8.0m. The span of the queen post truss in this section is about 9.0 m.

A slightly lower aisle was added to the nave on the southern side. Its floor-to-ceiling height is about 4.0 meters and its span is about 3.6 meters. Its single-pitched roof (queen post truss) rests on an added outer wall and on posts located at the nave's main columns (Figs. 1 and 5). Part of the log wall, up to the height of the aisle ceiling, has been disassembled (Fig. 6). The posts of the nave and aisle are connected to each other at some points, whereas the aisle roof structure is independent (queen post truss).

Another extension on the south side is the chapel, with a ceiling at the same level as that of the aisle. The chapel is topped with a gable roof with a ridge oriented perpendicularly to the chancel section. The roof, with a span of about 5.5 meters, has a collar beam truss strengthened with a ridge purlin. The body of the chapel from the south is closed with a triple-pitched roof topped with a small tower, with a ridge turret (Fig. 2a).

A sacristy is added to the north side of the chancel, with a ceiling height of about 2.5 meters and a span that varies from 3.3 to 3.6m. The sacristy roof is mono-pitched, with its ridge adjacent to the eaves of the chancel roof. In the wall between the chancel and the sacristy there are two doorways, one of which has been closed off.

Fig. 6. View of the wall between the nave and the aisle

Spatial rigidity of the structure

The outer walls of the individual parts running in parallel to the ridge on both sides of the building form a series of panels that provide high longitudinal rigidity to the entire structure. Although the lateral stiffness is different in each section of the building, it is far smaller than the longitudinal stiffness.

The newest part of the building on the west side is built with relatively short, mutually perpendicular walls, which makes its rigidity, both longitudinal and lateral, very high compared to older sections, including the nave. Although the choir section has a similar span as the nave, it is adjoined by a porch on one side and braced by the perpendicularly added gable wall of the aisle.

The body of the chancel on the eastern side is closed with a three-break wall and is further braced by an attached chapel on one side and an adjacent sacristy on the other. The walls of the additions surrounding the chancel are low, but the roof trusses and roofing form a rigid spatial structure that stiffens this part of the building laterally.

The lowest lateral rigidity is observed in the nave. The high and long side walls have no perpendicular stiffeners. Furthermore, the nave is considerably long and in the central part of the nave, all the load acting across the building must be carried by tall posts. On the north side, these posts are braced in the wall plane with log elements and plank sheathing, whereas on the south side, after the addition of a side aisle, the log wall was partially disassembled (Fig. 6). The posts lost their stiffening and the only reinforcement in their lower part is the additional pillars created with the new side aisle structure.

Measurements of the actual structure

Methodology

In order to fully diagnose the technical condition of the existing structure, the authors initiated a monitoring project consisting in measuring displacements at selected points. Due to the object's high historical value and unknown operating conditions, it was decided to use a combination of measurement methods, including static and dynamic measurements, allowing precise analysis of its behaviour. The observations were carried out in an integrated manner, i.e.

in addition to periodic geodetic measurements (static measurements, at selected time intervals), continuous monitoring (dynamic measurements, conducted in real time) was implemented [24].

The static measurements were carried out using the tachymetric method, at 1-month intervals. They included two reference points considered stable (unchanging) and 9 selected test points. The tachymetric method was based on measuring distances, directions and vertical angles. A Leica TCRP 1201+ one-second tachymeter was used, along with targets in the form of reflective foil shields, installed between 6.45 and 6.85 meters above floor level, just below a ceiling rising just over 7.0 meters above floor level. The height of 7.0m was considered a representative level for which displacements were calculated. The authors decided to control both the vertical and horizontal displacements. Due to possible settlement of the foundations, as well as the contraction and expansion of the structure, additional vertical displacement measurement points were introduced on the posts, just above the floor (Fig. 7).

The dynamic measurements were made using POSITAL FRABA ASG15 capacitive inclinometers with CANOPEN wired data transmission and a set of BWSENSING WF-WM400 biaxial wireless precise inclinometers made with MEMS technology. Initially, four inclinometers powered by electricity were installed at the facility. The readings were collected via a local Wi-Fi server and stored on disk.

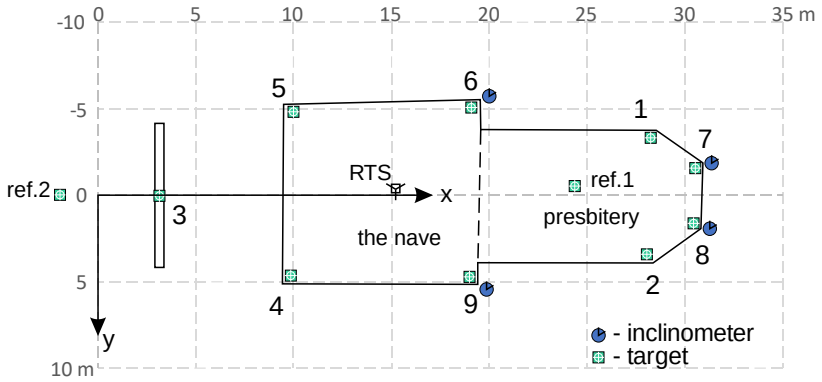

Fig. 7. Location of points for geodetic measurements

After initial tests, a recording frequency was set at every 10 seconds intervals, recording the extreme values from a given time interval. Based on the measured inclinations, the horizontal displacements of the structure at a height of 7.0 m were calculated using a simple relationship, assuming a hinge in the lower support of the column and the lack of flexural deformation along the length of the element, i.e.:

$$u = h \cdot \tan(\alpha), \tag{1}$$

where: u is the value of horizontal displacement at hight h and α is the inclination angle of the post. This provided values for the two components of displacement: ux in the X axis direction and uy int the Y axis direction, at the same level as the installed tachymetric targets.

To obtain a set of representative measurement data, the authors established six measurement points and four locations of biaxial inclinometers. To control the accuracy of measurements, they determined an additional point for static measurements and inclinometer readings. Based on these, they planned to calculate the correlation coefficients between gusts of wind and the displacement readings. They also checked the relationship between the results obtained from the static measurements and the displacements obtained from the computational model, which was based on inclinometer readings (dynamic measurements).

Outside, a SENCOR 12500 WiFi weather station including a set of sensors: two thermometers, a barometer, a wind gauge and a precipitation meter, was installed about 5 meters from the building and 5 meters above the church floor level. A thermometer located inside the building was also connected to the weather station. Using the Weathercloud service, it was possible to remotely view station readings recorded at intervals, every 10 minutes. The acquired data were used to compare the weather changes with the results of inclinometer measurements [25].

Since it was possible to read the measurements from the weather station at 10-minute intervals, the same frequency of recording was adopted for all other measurements. In this way, for each measured value, a database of 144 readings per day, 1008 readings per week and about 4400 readings per month was obtained. The resulting large dataset gave a good illustration of the structure's response to varying climatic loads. The obtained information was used to validate the computational model of the structure as well as to assess its technical condition.

Measurement results

Table 1 and 2 summarize the results of measurements that were taken from March 2021 to January 2022 at ten points: points 1 to 9 and point 3a (under point 3 in Fig. 7). Measurements taken on February 27 (survey "0") were treated as reference values.

Table 1. Results of measurements of static displacement increments at selected points (March - July 2021)

	Increments determined in relation to the reference measurement: $D_n - D_0$														
Survey / Date	4 / 25-3-2021			5 / 22-4-2021			6 / 18-5-2021			7 / 19-6-2021			8 / 21-7-2021		
Increment	dx	dy	dz	dx	dy	dz	dx	dy	dz	dx	dy	dz	dx	dy	dz
Point															
1	0.3	-0.2	0.7	-1.1	-0.3	0.5	-0.1	0.0	1.4	-0.5	-0.1	1.4	-1.0	0.0	0.8
2	-0.7	0.2	0.5	-1.5	0.1	0.4	-1.4	1.0	0.6	-1.8	0.6	0.5	-1.5	0.9	0.3
3	-0.9	-0.1	1.8	-1.8	-0.8	1.8	-2.1	0.1	1.8	-1.2	-0.2	2.1	-2.2	0.8	0.1
3a	-0.4	0.2	0.6	-1.3	-0.4	0.7	-1.5	0.5	0.7	-1.0	0.4	1.2	-1.5	0.5	0.3
4	-0.4	-0.5	2.2	-0.8	-0.2	1.4	-1.4	0.3	1.1	-1.2	0.0	1.2	-1.7	0.1	0.7
5	-0.7	-1.7	0.2	-0.9	-1.6	0.2	-1.6	-1.7	0.0	-1.2	-2.2	0.1	-1.1	-1.8	0.3
6	-0.5	-2.5	0.0	-0.9	-1.6	-0.1	-1.1	-2.5	-0.4	-1.2	-1.7	-0.2	-1.1	-1.3	0.0
7	-0.5	-1.7	0.4	-0.6	-1.7	0.3	-0.2	-2.5	0.1	-0.2	-1.8	0.1	-0.4	-1.8	0.1
8	-0.3	-2.2	0.1	-0.9	-1.7	0.5	-0.6	-2.5	0.1	-0.2	-1.9	-0.3	-0.5	-2.0	-0.5
9	-0.9	-1.1	0.3	-1.1	-1.1	0.4	-0.6	-1.1	0.3	-1.2	-1.5	0.4	1.4	0.0	0.6
Mean value	-0.5	-1.0	0.7	-1.1	-0.9	0.6	-1.1	-0.8	0.6	-1.0	-0.8	0.6	-1.0	-0.5	0.3
Standard deviation	0.4	1.0	0.7	0.4	0.7	0.6	0.7	1.4	0.7	0.5	1.1	0.8	1.0	1.1	0.4

	Increments of displacement in relation to the previous measurement: $D_n - D_{n-1}$														
Point															
1	0.3	-0.2	0.7	-1.4	-0.1	-0.2	1.0	0.3	0.9	-0.4	-0.1	0.0	-0.5	0.1	-0.6
2	-0.7	0.2	0.5	-0.8	-0.1	-0.1	0.1	0.9	0.2	-0.4	-0.4	-0.1	0.3	0.3	-0.2
3	-0.9	-0.1	1.8	-0.9	-0.7	0.0	-0.3	0.9	0.0	0.9	-0.3	0.3	-1.0	1.0	-2.0
3a	-0.4	0.2	0.6	-0.9	-0.6	0.1	-0.2	0.9	0.0	0.5	-0.1	0.5	-0.5	0.1	-0.9
4	-0.4	-0.5	2.2	-0.4	0.3	-0.8	-0.6	0.5	-0.3	0.2	-0.3	0.1	-0.5	0.1	-0.5
5	-0.7	-1.7	0.2	-0.2	0.1	0.0	-0.7	-0.1	-0.2	0.4	-0.5	0.1	0.1	0.4	0.2
6	-0.5	-2.5	0.0	-0.4	0.9	-0.1	-0.2	-0.9	-0.3	-0.1	0.8	0.2	0.1	0.4	0.2
7	-0.5	-1.7	0.4	-0.1	0.0	-0.1	0.4	-0.8	-0.2	0.0	0.7	0.0	-0.2	0.0	0.0
8	-0.3	-2.2	0.1	-0.6	0.5	0.4	0.3	-0.8	-0.4	0.4	0.6	-0.4	-0.3	-0.1	-0.2
9	-0.9	-1.1	0.3	-0.2	0.0	0.1	0.5	0.0	-0.1	-0.6	-0.4	0.1	2.6	1.5	0.2
Mean value	-0.5	-1.0	0.7	-0.6	0.0	-0.1	0.0	0.1	0.0	0.1	0.0	0.1	0.0	0.4	-0.4
Standard deviation	0.4	1.0	0.7	0.4	0.5	0.3	0.5	0.7	0.4	0.5	0.5	0.2	1.0	0.5	0.7

The red colour in the tables indicates displacement increments exceeding the value of 2mm. The results shown in the tables have a variation in all components of displacement, between successive measurements, ranging from 0.4 to 0.6mm. The exception is the error in the

lateral direction of 1.2mm, which may indicate the building's tendency to lean laterally. Overall, the detected inclinations do not exceed 1.5mm in the X-axis direction and 3.6mm in the Y-axis direction. The measured values are relatively small, inclinations along the length of the building may indicate structural separation, while lateral inclination, the largest values of which are in the chancel, may be the result of thermal deformation.

The vertical displacements are within measurement error, hence there is no reason to suspect that there were any settlements in the building.

During continuous monitoring (dynamic measurements), the inclinations of structural elements were recorded at selected points. The angular values were used to calculate the horizontal displacements at a height of 7m, after taking into account corrections due to the lack of plastic deformation of the tested structure. This assumption was made on the basis of zero displacement of points measured with a tachymeter under steady-state weather conditions, i.e. when there was no wind, the temperature ranged from 5 to 10°C and sunshine was low.

Table 2. Results of static displacement measurements at selected points (March 2021 – January 2022)

Increments determined in relation to the reference measurement: $D_n - D_0$															
Survey No./ Date	9 / 27-8-2021			10 / 25-9-2021			11 / 27-10-2021			12 / 25-11-2021			13 / 30-12-2021		
Increment	dx	dy	dz	dx	dy	dz	dx	dy	dz	dx	dy	dz	dx	dy	dz
Point															
1	-0.1	-0.3	0.5	-0.5	0.5	0.1	-0.1	0.3	0.2	1.3	0.6	0.5	1.2	0.8	0.5
2	-1.7	0.4	-0.5	-0.4	1.3	-0.3	-0.7	0.9	-0.4	0.2	0.7	-0.2	0.7	1.2	0.0
3	-2.0	0.9	-0.3	-1.0	2.0	-0.3	-1.4	2.1	-0.5	-0.2	1.7	-0.5	0.2	2.5	-0.3
3a	-1.2	1.2	-0.3	-0.3	1.7	-0.4	-0.8	1.2	-0.4	0.7	0.7	-0.7	0.9	1.3	-0.4
4	-2.1	0.1	0.5	-1.3	1.4	0.9	-1.4	1.0	0.5	-0.9	0.5	0.8	-0.1	1.6	0.9
5	-1.2	-2.0	0.3	-0.8	-0.4	0.0	-0.8	-1.6	0.4	-0.8	-1.5	0.3	-0.1	-0.1	0.7
6	-0.9	-1.7	-0.2	-0.4	-0.3	-0.2	-1.0	-2.5	0.0	-1.6	-2.9	0.7	-1.2	-1.2	0.4
7	-0.8	-1.9	0.2	-0.1	-1.5	0.1	0.0	-1.6	0.5	-0.5	-2.2	0.6	-0.9	-1.5	0.7
8	-1.0	-2.0	0.0	-0.1	-1.2	0.3	-0.5	-2.5	0.2	-0.4	-3.2	0.1	-0.7	-1.9	0.3
9	-1.0	-0.9	-0.3	0.9	1.4	-0.7	-0.1	-1.3	0.4	-0.2	-1.2	0.1	0.3	-0.5	0.4
Mean value	-1.2	-0.6	0.0	-0.4	0.5	-0.1	-0.7	-0.4	0.1	-0.2	-0.7	0.2	0.0	0.2	0.3
Standard deviation	0.6	1.2	0.4	0.6	1.3	0.4	0.5	1.7	0.4	0.8	1.7	0.5	0.8	1.5	0.4
Increments of displacement in relation to the previous measurement: $D_n - D_{n-1}$															
Point															
1	0.9	-0.3	-0.3	-0.4	0.8	-0.4	0.4	-0.2	0.1	1.4	0.3	0.3	-0.1	0.2	0.1
2	-0.2	-0.5	-0.8	1.3	0.9	0.2	-0.3	-0.4	-0.1	0.9	-0.2	0.2	0.5	0.5	0.2
3	0.2	0.1	-0.4	1.0	1.1	0.0	-0.4	0.1	-0.2	1.2	-0.4	0.0	0.4	0.9	0.2
3a	0.3	0.7	-0.6	0.9	0.5	-0.1	-0.5	-0.5	0.0	1.5	-0.5	-0.3	0.2	0.6	0.3
4	-0.4	0.0	-0.2	0.8	1.3	0.4	-0.1	-0.4	-0.4	0.5	-0.5	0.3	0.8	1.1	0.1
5	-0.1	-0.2	0.0	0.4	1.6	-0.3	0.0	-1.2	0.4	0.0	0.1	-0.1	0.7	1.4	0.3
6	0.2	-0.4	-0.2	0.5	1.4	0.0	-0.6	-2.2	0.2	-0.6	-0.4	0.7	0.4	1.6	-0.3
7	-0.4	-0.1	0.1	0.7	0.4	-0.1	0.1	-0.1	0.4	-0.5	-0.6	0.1	-0.4	0.7	0.1
8	-0.5	0.0	0.5	0.9	0.8	0.3	-0.4	-1.3	-0.1	0.1	-0.7	-0.1	-0.3	1.4	0.3
9	-2.4	-0.9	-0.9	1.9	2.3	-0.4	-1.0	-2.7	1.1	-0.1	0.1	-0.3	0.5	0.7	0.3
Mean value	-0.2	-0.2	-0.3	0.8	1.1	0.0	-0.3	-0.9	0.1	0.4	-0.3	0.1	0.3	0.9	0.2
Standard deviation	0.9	0.4	0.4	0.6	0.6	0.3	0.4	0.9	0.4	0.8	0.3	0.3	0.4	0.4	0.2

The diagrams (Figs. 8 and 9) show the values of displacements calculated from the recorded inclinations at measurement points No. 6 and No. 9 during strong winds, on February 17, 2023 (12:00 p.m. – 12:00 a.m.).

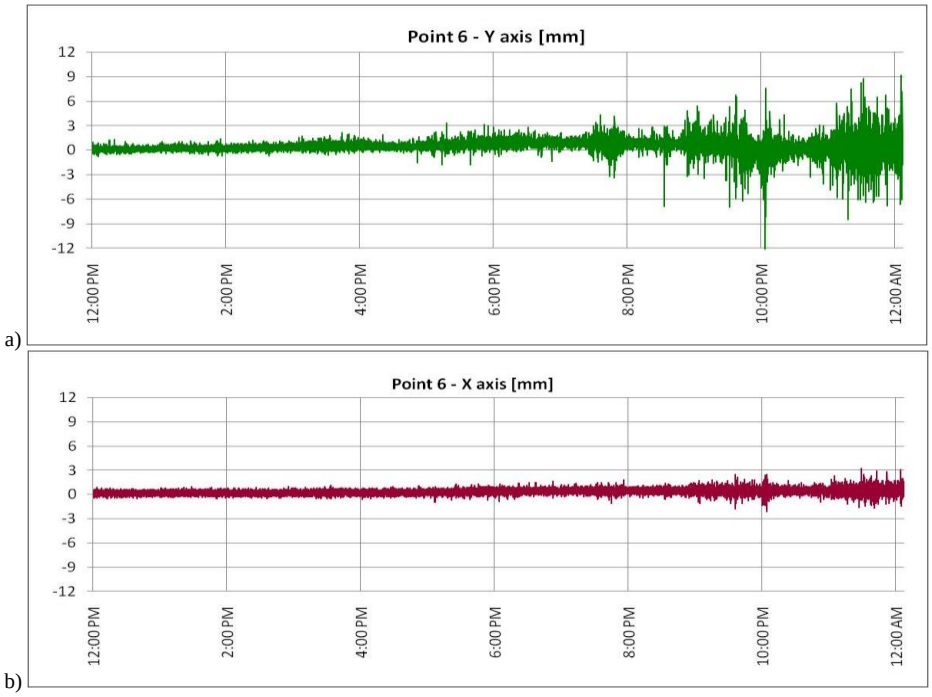

Fig. 8. Diagrams of displacements of the structure at point No. 6 on February 17, 2023 during strong winds: a) across the building, Y axis direction, b) along the building X axis direction.

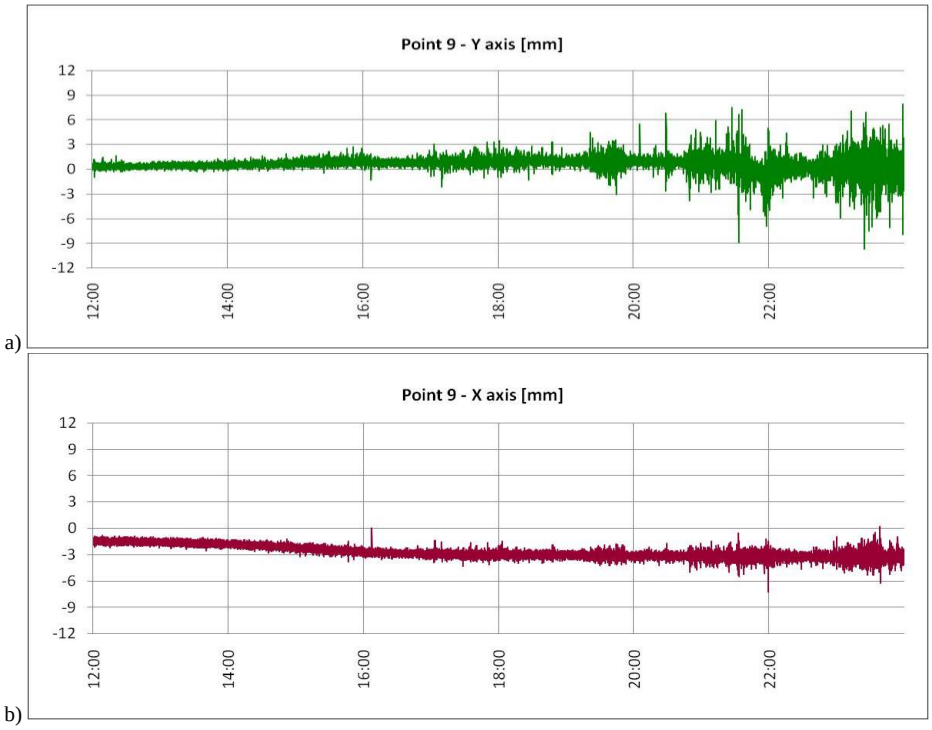

Fig. 9. Diagrams of displacements of the structure at point No. 9 on February 17, 2023 during strong winds: a) across the building, Y axis direction, b) along the building X axis direction

The diagrams of measured deformations (Figs. 8 and 9) show a significant increase in the values of the displacement across the building (Y axis) in the evening, which, however, did not exceed the value of 12mm. The displacement oscillations were the result of load variation, the wind push was irregular and stronger wind gusts were short-lived, even impulsive. Figure 10 shows the measurements of the average wind speed, its speed during gusts and the mean direction of the measured wind. The measurements come from the weather station situated in the neighbourhood of the building.

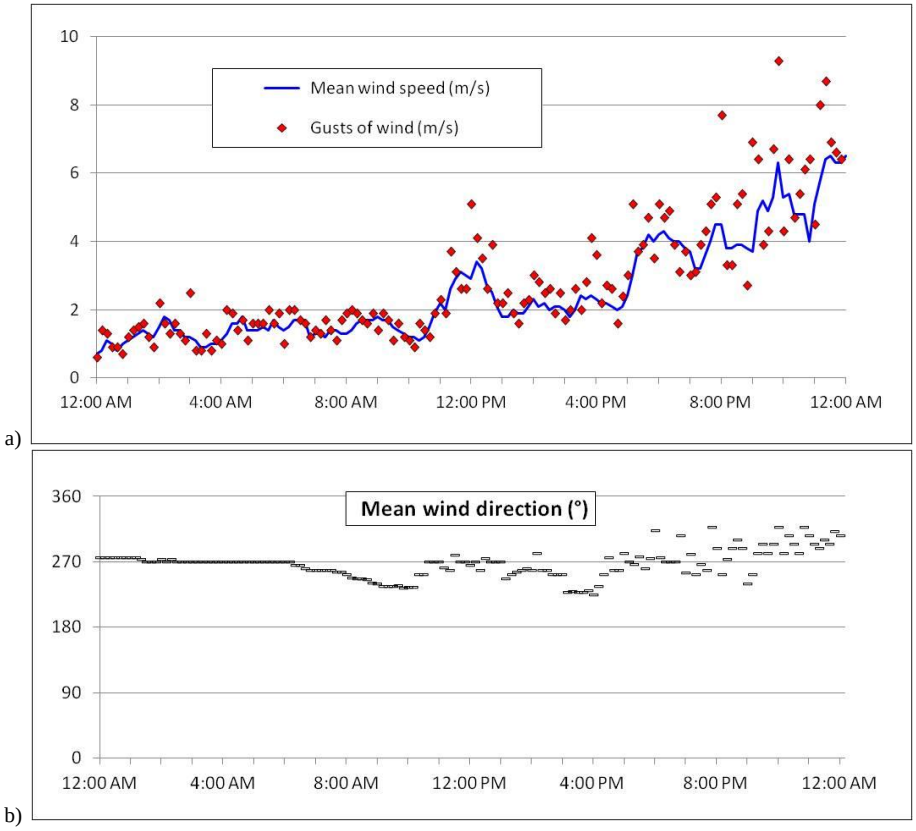

Fig. 10. Wind measurement on February 17, 2023: a) wind speed, b) wind direction.

The wind speed increased in the second part of the day and the gusts became stronger. According to the weather station's indications, a westerly wind dominated throughout the day.

Dynamic analysis of the structure

Methodology

Dynamic tests including acceleration measurements at selected points of the structure and modal analyses of selected structural elements were performed using Dewesof measuring equipment:

- An Endevco 100mV/g uniaxial accelerometer (42A16-1032) and a Dytran 100mV/g triaxial accelerometer (3263A8T) were used to measure the dynamic response of the structure;
- A 50mV/lbf modal hammer (2302-50) was used to excite vibrations;
- a SIRIUS 8xACC analyser (DEW_SIRIUS 8xACC) was used for data acquisition.

DewesoftX software, version 2021.6 (Copyright © 2000-2023 Dewesoft) was used for data processing and analysis of measured values. The SIRIUS analyser had eight analogue inputs (+/-10V), a sampling capacity of up to 200kHz per channel and 2x24-bit analog-to-digital conversion.

The tests were scheduled for a period of significant loads from high-speed winds combined with stronger gusts. Accelerations were measured using a triaxial accelerometer mounted on a selected structural element. The recorded signal was subjected to a fast Fourier transform (FFT) procedure, based on which the dominant free vibration frequency was determined. After filtering, i.e. after cutting off the values associated with the higher vibration frequencies, the signal was subjected to the integration procedure twice. In this way, the approximate amplitudes of the displacements calculated from the recorded accelerations were determined.

The second type of dynamic measurements was used to carry out a modal analysis. For this purpose, a triaxial accelerometer was mounted on the tested structural element at a selected point. Next, based on a predetermined scheme, a dynamic pulse was applied at pre-selected points along the test element. Using a modal hammer, the force and time of application of the dynamic pulse at one point were measured and recorded simultaneously with the acceleration measured at another point.

The modal analysis software made it possible to determine the transmittance of the signal, the natural frequency of the tested element and the associated mode of vibration. Since a small modal hammer cannot excite the entire structure, the modal analysis focused on a selected element of the structure, where vibrations were excited locally.

Measurement of accelerations at a selected point

The tests were performed on February 17, 2023, during a period when the west wind was blowing at speeds of up to 10m/s, with gusts of up to 20m/s (according to the official weather station). The accelerations were measured with a triaxial accelerometer mounted on a nave post located in the northern wall (Fig. 11). The sensor was mounted at a height of about 6.0m from floor level.

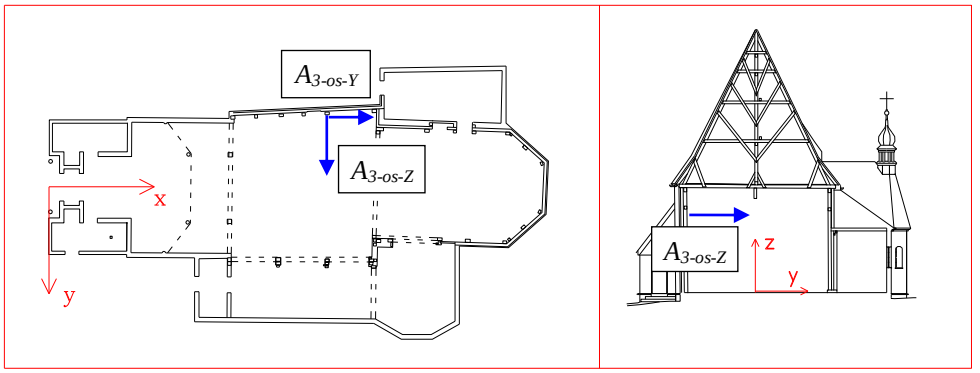

Fig. 11. The position of the measurement point and directions of measured acceleration: along the building ($A_{3\text{-}os\text{-}Y}$) and across the building ($A_{3\text{-}os\text{-}Z}$)

Ten-second fragments of the signals measured in two perpendicular directions are shown in figure 12, where the acceleration values along the building ($A_{3\text{-}os\text{-}Y}$) are in red, while the accelerations recorded across the building ($A_{3\text{-}os\text{-}Z}$) are in blue.

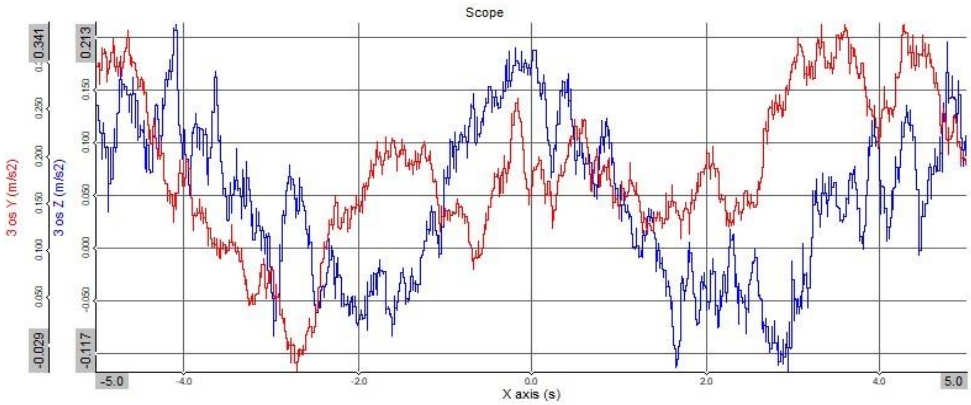

Fig. 12. Diagram of accelerations along the building ($A_{3\text{-}os\text{-}Y}$ in red) and across the building ($A_{3\text{-}os\text{-}Z}$ in blue)

After performing a Fast Fourier Transform (FFT), a graph of the signal in the frequency domain was obtained (Fig. 13). Based on the graph obtained, it can be concluded that the dominant movement of the structure was at very low frequencies. This type of movement can hardly be considered a harmonically time-varying oscillation. Rather, the observed regularity was due to a load that operated periodically. The gusts of wind caused the short-lasting pressure that was repeated over time. The displacements were quasi-static, caused by the action of a short-term variable load. The structure moved during gusts of wind and returned to its equilibrium position.

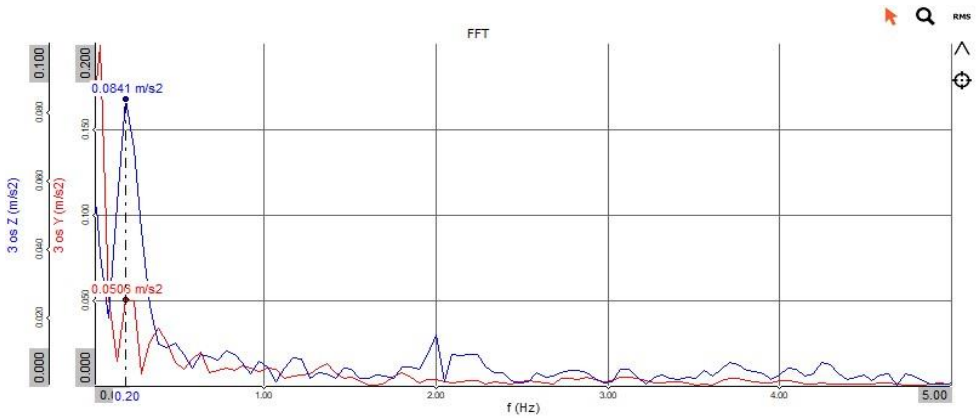

Fig. 13. Fast Fourier Transform (FFT) of the recorded acceleration: along the building ($A_{3\text{-}os\text{-}Y}$) - red color, across the building ($A_{3\text{-}os\text{-}Z}$) - blue color

The recorded acceleration signals were subjected to further transformations. First, a low-pass filter was used to cut off the acceleration values associated with vibration frequencies that were higher than 0.5Hz. The filtered signal was then subjected to the integration procedure twice. The displacement amplitudes obtained in this way should be treated as approximate values, since the recorded signal cannot be regarded as harmonic oscillations. It is worth noting that the calculated amplitudes of displacement in the analyzed time interval did not exceed 6mm (Fig. 14).

No distinct oscillations with frequencies higher than 0.2Hz were recorded during vibration measurements of the wind-loaded structure. Therefore, it can be concluded that the structure was not dynamically excited during the measurements.

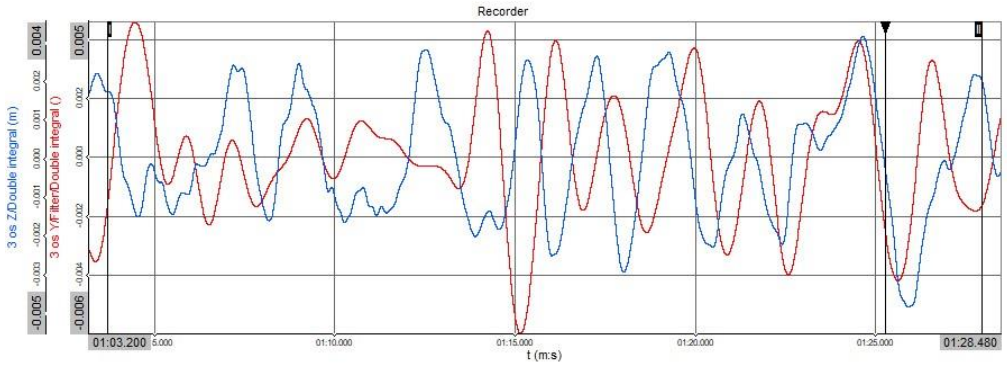

Fig. 14. Double-integrated acceleration signal: along the building (*3-os-Y*) - red color, across the building (*3-os-Z*) - blue color

The loading of an object by forces induced by wind gusts can be used to carry out a so-called operational modal analysis. In this analysis, the response of a structure induced by dynamic forces occurring during its regular operation is measured. However, in this case, the response of the structure, i.e. its wind-induced deformation was relatively slow. After the load vanished, the structure returned to the equilibrium position and the whole process of loading and unloading had the character of creep motion. On the other hand, the graph in figure 12 shows one complete cycle with a period of about 5 s, which may make dynamic analysis reasonable.

Numerical model of the structure

Design assumptions

The building's main load-bearing structure is a spatial bar system braced by panels (diaphragms) in the planes of the walls, in the planes of the floors and ceilings and in the planes of the roof slopes. In the wall planes, the stiffening is provided by masonry infill (half-timbering) and log wall elements reinforced by external plank sheathing. In the floor planes, stiffening is provided by ceiling planking and attic floors.

In the calculation software, the structure of the building was modelled as a bar structure, in which the members are straight and their cross-sections are constant along their length (prismatic bars). In addition, in the newer section situated on the west side, featuring the porch and the choir, the authors assumed that the bar structure is stiffened by masonry walls. With relatively short and mutually perpendicular walls, this part showed greater spatial rigidity in comparison to the older section with the nave and the chancel (Fig. 15).

After the modelling of the load, static and dynamic analysis of the structure was performed. The extreme nodal displacements, internal forces and stresses in the elements of the structure were determined. Moreover, displacements were determined for those nodes of the model for which measurements were carried out in the actual structure. The displacement values determined at the control points were one of the comparison criteria in the parametric analysis and in the sensitivity analysis.

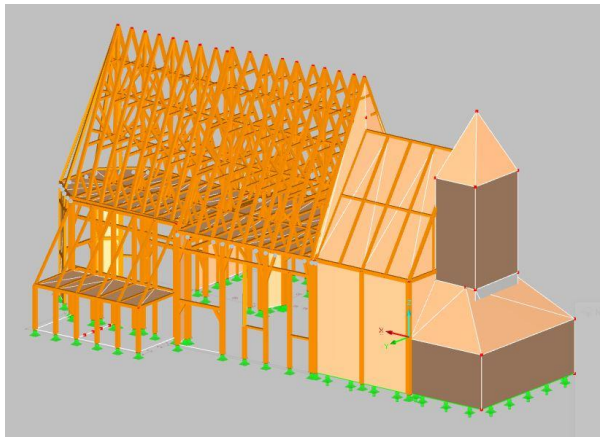

Fig. 15. View of the computational model of the structure (north-west direction)

Spatially stiffening panels

The authors carried out static and dynamic analyses for several calculation models differing in the number and arrangement of stiffening panels. The first model was built with bars alone and in each subsequent model stiffening panels were added, both in the floor planes and in the wall planes. In each case, the displacements induced by south-east wind were determined at the control nodes. The analyses were conducted for the following models:

- SE-S-0 – initial model: bar structure,
- SE-S-1 – bar model with ceiling panels (*T1* in Fig. 16) in the nave and chancel,
- SE-S-2 – model SE-S-1 increased with ceiling panels in the aisle (*T2* in Fig. 16), in the chapel and the sacristy,
- SE-S-3 – model SE-S-2 with added wall panels in the chancel (*T3* in Fig. 16),
- SE-S-4 – model SE-S-3 plus wall stiffening panels in the chapel (*T4* in Fig. 16),
- SE-S-5 – model SE-S-4 plus two short stiffening side walls at the junction of the nave and the chancel (*T5* in Fig. 16).

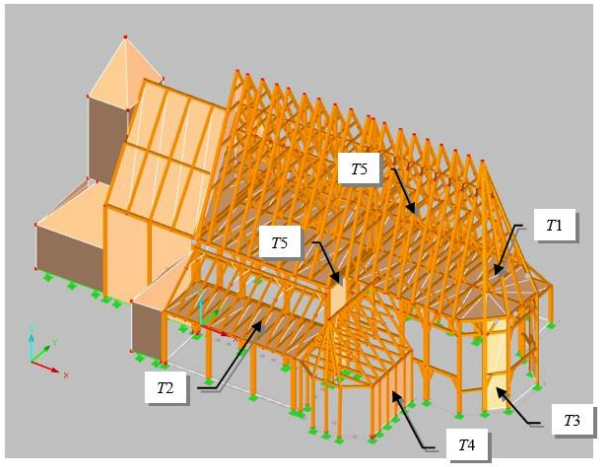

Fig. 16. Computational model with marked stiffening panels, view from the southeast direction

The results of the calculations are summarized in Table 3 and presented in the graphs in figure 17.

Table 3. Displacements at selected nodes in the subsequent models induced by southeast wind

Model	Horizontal displacements [mm]					
	Max.		Node 128 (point No. 6)		Node 16 (point No. 8)	
	Longitudinal X-axis	Lateral Y-axis	Longitudinal X-axis	Lateral Y-axis	Longitudinal X-axis	Lateral Y-axis
SE-S-0	3.1	**17.5**	**1.7**	**16.5**	0.2	**12.2**
SE-S-1	1.9	9.2	**1.7**	6.6	**0.5**	8.9
SE-S-2	**3.2**	8.6	1.6	6.1	**0.5**	8.4
SE-S-3	2.9	6.0	1.3	5.1	0.3	2.6
SE-S-4	2.9	5.6	1.2	4.8	0.2	2.4
SE-S-5	1.7	3.1	0.4	2.1	0.1	1.6

Displacements induced by the southeast wind were calculated in two directions: along the church (along the X axis) and across the building (along the Y axis). Selected values are presented, that is, the displacements calculated for node No. 128, which corresponds to the actual measurement point No. 6 (Fig. 7) and the values calculated for node No. 16, which corresponds to measurement point No. 8 (Fig. 7). The measurements of the actual displacements were discussed in an earlier chapter, the locations of measurement points 6 and 8 are shown in figure 7, while Table 3 and figure 17 show the results of numerical calculations.

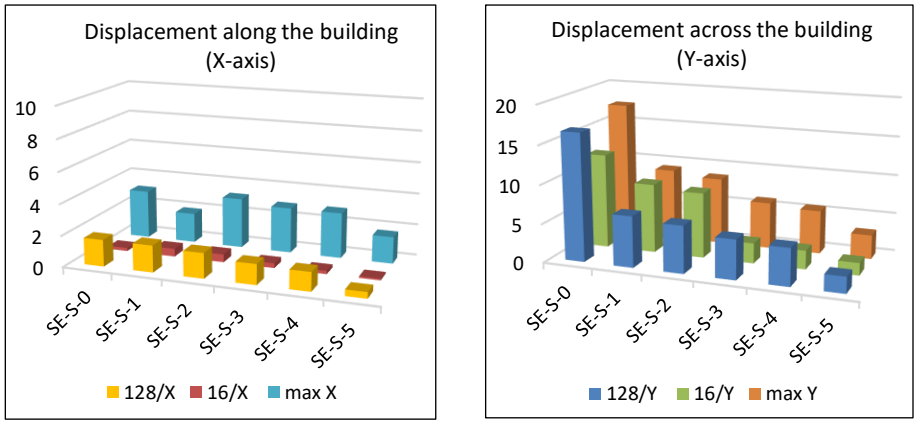

a) b)

Fig. 17. Displacements at selected nodes (No. 128 and No. 16) of the analysed structural models: a) along the building, b) across the building

Figure 18 shows the deformations in the model in which the *T5* panels at the junction of the chancel and nave are not included (Fig. 18a, model SE-S-4) and the model in which these panels are included (Fig. 18b, model SE-S-5).

Comparing the magnitudes of the displacements in the two models, one can notice the importance of the short stiffening walls between the chancel and the nave, which were labeled *T5* in figure 16.

Next, the same models, in which stiffening panels were successively added, were loaded with wind blowing from the Northwest. The results of the calculated displacements are summarised in Table 4. For this kind of load, the displacements in selected nodes were also calculated in two directions: along and across the building.

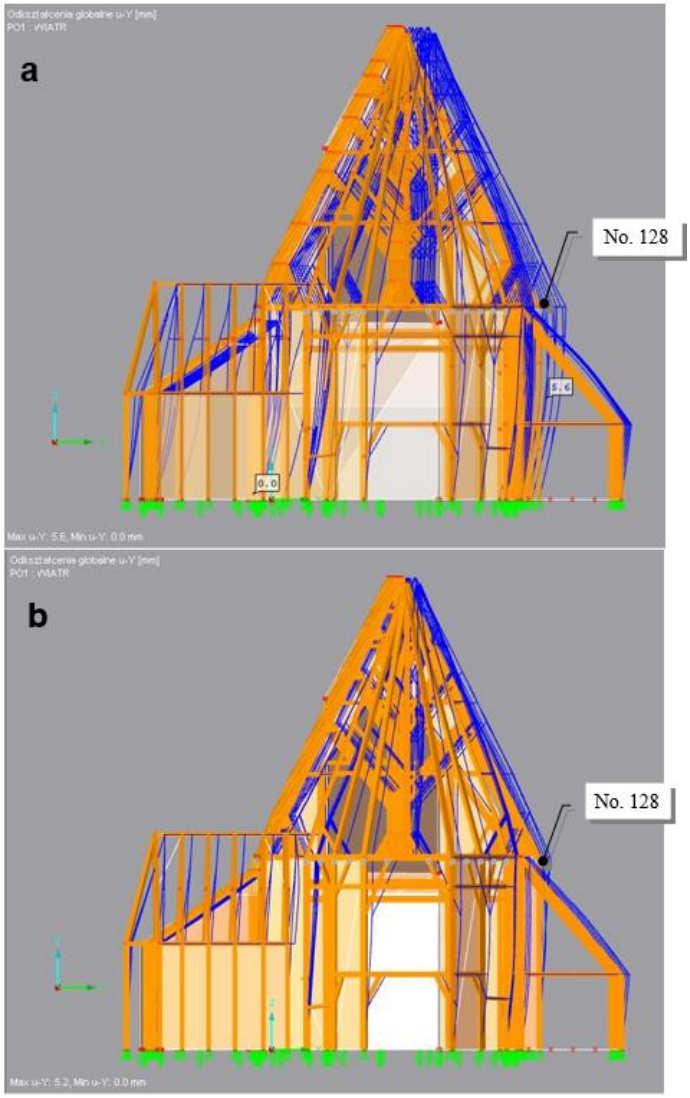

Fig. 18. Structural deformation caused by southeast wind: a) SE-S-4 model, without *T5* panels, b) SE-S-5 model, containing *T5* panels

Table 4. Displacements at selected nodes in the subsequent models induced by northwest wind

Model	Horizontal displacements d_i [mm]					
	Maximum		Node 128 (point No. 6)		Node 16 (point No. 8)	
	Longitudinal X-axis	Lateral Y-axis	Longitudinal X-axis	Lateral Y-axis	Longitudinal X-axis	Lateral Y-axis
NW-S-0	**7.6**	**29.6**	**3.5**	**26.9**	**2.8**	**10.3**
NW-S-1	3.9	13.8	3.2	12.7	2.0	9.4
NW-S-2	6.3	13.2	3.0	11.7	2.0	8.4
WN-S-3	6.0	12.7	2.6	10.8	2.2	3.2
NW-S-4	6.1	12.3	2.4	10.2	2.1	2.9
NW-S-5	3.5	8.6	0.7	4.5	1.2	1.3

As expected, the stiffening panels have a major impact on the spatial rigidity of the post-and-beam structure. However, based on the above analysis, the authors concluded that the stiffening panels in the short sections of the walls between the nave and the chancel are the most important, as their inclusion in the calculations leads to the greatest reduction in displacements. In the actual construction, these short walls are weakened, at the junction of two perpendicular walls the logs are not well connected, gaps are visible (Fig. 19). This means that the walls are not rigidly connected to each other, the elements can displace independently and the mentioned walls do not act as stiffening panels. Furthermore, the rood beam on the right side, is broken at the notch (a narrowed area), which confirms the supposition that in this plane the structure is not properly stiffened (Fig. 19).

Fig. 19. Fragments of short log walls at the junction between the nave and chancel

Impact of defects and weaknesses in the material

The next analysis aimed to determine the impact of the weakened elements of the frame structure on the stability of the entire system. There are weaknesses in many elements of the timber post-and-beam structure, which are the result of numerous modifications, these are undercuts, cuts or narrowing of the elements at a longer range. In the post-and-beam wall elements there are remnants of old carpentry joints: notches, tenons and dowel holes, which considerably reduce the active cross-section area and thus reduce the load-bearing capacity of the element itself (Fig. 20).

Particularly dangerous in the case of flexural elements are defects in the area of the outermost fibers of the active section, i.e. in areas of extreme normal stresses. A reduction in the cross-sectional area directly affects the load-bearing capacity of the element, but the influence of a weakened element on the stability of the entire structure requires a separate analysis.

Weaknesses in the actual structure occur at various points, their distribution is random along the length of the element and in the object space. Thus, their inclusion in the calculation model required some simplifications and generalizations. It was assumed that smaller cross-sectional dimensions occur along the entire length of the selected element.

Fig. 20. Notches and dowel holes weakening the columns in the north wall of the nave

The authors conducted numerical analyses for several computational models of the structure, in which weaknesses were assumed in selected groups of elements:

- SE-S-0-w1n – bar structure with weakened columns of the nave,
- SE-S-0-w2p – bar structure with weakened columns of the chancel,
- SE-S-0-w3r – bar structure with weakened roof rafters,
- SE-S-5-w1n – model with all stiffening panels and weakened nave columns,
- SE-S-5-w2p – model with all stiffening panels and weakened chancel columns,
- SE-S-5-w3r – model with all stiffening panels and weakened roof rafters.

The results of numerical calculations, the values of extreme displacements at nodes and the values of extreme stresses in selected elements are summarised in Table 5. For comparison, the values of displacements and stresses for the bar model without weaknesses (model SE-S-0) and for the model without weaknesses but with all the stiffening panels (model SE-S-5) are also given.

Table 5. Displacements and stresses in structural models without and with weakened elements

	Maximum horizontal displacements d_i [mm]		**Extreme stresses in the posts σ_i [MPa]**	
Model	**Longitudinal X-axis**	**Lateral Y-axis**	**Nave**	**Chancel**
SE-S-0	3.1	17.5	1.547	3.682
SE-S-0-w1n	3.8	18.9	1.828	3.740
SE-S-0-w2p	3.6	**22.0**	1.848	**8.722**
SE-S-0-w3r	**5.0**	18.3	1.584	3.699
SE-S-5	1.7	3.1	0.941	0.821
SE-S-5-w1n	1.9	10.2	**1.883**	0.848
SE-S-5-w2p	1.8	3.4	0.921	0.965
SE-S-5-w3r	1.7	3.4	0.946	0.858

The results of the analyses showed that the load-bearing capacity of the columns in the chancel walls is very important, as the structure is sensitive to their weakening. In the bar model without stiffening panels, the weakening of the chancel columns (model SE-S-0-w2p) results in a more than twofold increase in stress values in them. In contrast, in the models with stiffening panels and weakening, the posts in the nave have a greater influence on the performance of the entire structure. The analyses show that their weakening (model SE-S-5-w1n) causes and over threefold increase in displacement and twofold increase in stress. Figure 21 shows the distribution of stress in the nave columns (Fig. 21a) and chancel columns (Fig. 21b) for the SE-S-5-w1n model.

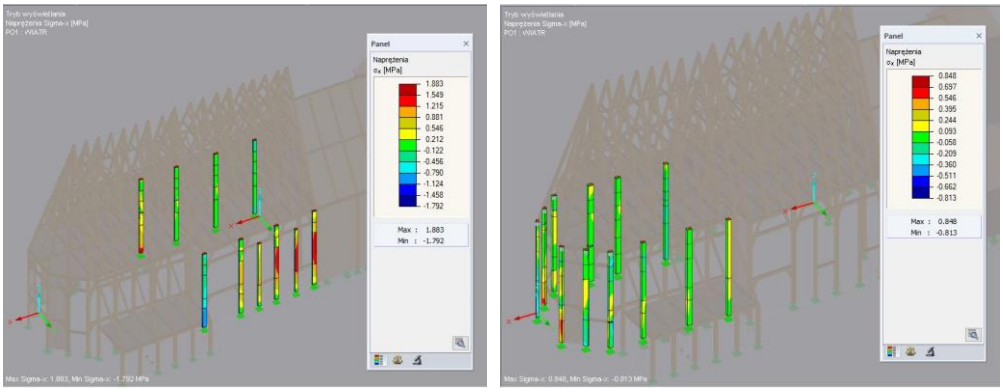

a) b)

Fig. 21. Distribution of wind-induced stresses, in the posts: a) of the nave, b) of the chancel

Modelling the wall/roof connection

Another important factor that weakens the structure is cavities caused by the biological corrosion of wood. The greatest degradation of wooden elements occurred in the supports of the frame structure. In some places, the sill plate has completely decayed and no longer serves its purpose (Fig. 22).

The degradation of the sill plates and post supports was the likely cause of the whole construction leaning to the west and the reason for the reconstruction of the church in the early 20th century. The corroded bottom parts of some of the posts were cut off and replaced with brick plinths (Fig. 23). In addition, new sill plates were inserted along some of the walls.

In the calculation model, it was assumed that the columns of the frame structure are hinged support. The subsequent analysis concerned the impact of the method of joining the walls with the roof. The upper beams in the walls with the posts, angle braces and struts form a stiffening panel in the plane of the wall, while the ceiling joists, which reach the plane of the wall perpendicularly, together with the rafters form a spatial roof truss. The actual connection between the roof and the wall is elastic and is neither fully rigid nor fully hinged.

The numerical calculations investigated two models for the wall-roof connection, both for the nave and the chancel. The SE-Png-5 model assumed that the connection of the posts in the nave with the roof is hinged, while the SE-Ppr-5 model assumed that the connection of the posts in the chancel with the roof is hinged. The results were then compared with those obtained for the model where these connections are rigid (model SE-S-5). Selected results of the calculations, i.e. displacements of the structure and stresses in selected elements, are summarized in Table 6.

Fig. 22. Degraded sill plate in the chancel

Fig. 23. A multi-branched column set on a brick plinth

Table 6. Displacements and stresses in structural models for rigid and hinged connections at the wall-roof junction

Model	Maximum horizontal displacements d_i [mm]		Extreme stress in the posts σ_i [MPa]	
	Longitudinal X-axis	Lateral Y-axis	Nave	Chancel
SE-S-5 (rigid)	1.7	3.1	0.941	0.821
SE-Png-5 (nave – hinge)	1.7	3.1	0.937	0.803
SE-Ppr-5 (chancel – hinge)	1.7	3.1	0.940	0.826

The hinged connection of the wall structure to the roof structure has little impact on the global performance of the analysed system. The differences in the results of the obtained stresses are negligible and the maximum values of displacements are the same in all analyzed models.

Numerical dynamic analysis

Another area of research was the dynamic analysis of selected numerical models, for which the dynamic characteristics of the structure, i.e. natural frequencies and vibration modes, were determined. In such a complex and sophisticated structure, the calculated free vibration frequencies may refer only to a part of the building, which means that the dominant vibrations will occur only in one element, such as a column, or in a separate part, such as a wall. To be able to assess whether a given resonant frequency excites the entire structure or only a part of it, it is necessary to analyze the vibration mode associated with that frequency. Vibrations at the resonant frequency of a fragment of a structure are dangerous only for that fragment, which means that the area of possible destruction is limited. For structural safety, the most important are those resonant frequencies during which the entire body of the building is excited to vibrate. In the structure under study, the only dynamic load that can induce vibration of the entire building is the action of wind. The results of the dynamic calculations are summarised in Table

7, which presents the fundamental (lowest) resonant frequencies for the selected models, during which the entire structure was excited.

Table 7. Fundamental natural frequencies of selected models of the structure

Model	SE-S-0	SE-S-1	SE-S-2	SE-S-3	SE-S-4	SE-S-5
f_1 [Hz]	1.883	2.410	2.495	2.925	3.050	4.164
ω_1 [rad/s]	11.834	15.143	15.674	18.377	19.164	26.165

The first, fundamental vibration frequency for the bar model, which does not include stiffening panels (model SE-S-0), is related to the mode in which the entire building body moves laterally (Fig. 24). This means that the lateral stiffness in this model is the lowest. Moreover, the stiffness of the older part (i.e., the nave and chancel) is significantly lower than that of the newer part of the building.

The displacements shown in Figure 24 are in one direction, all parts of the building are in phase with each other. Subsequent vibration modes for this model are also dominated by lateral displacements over the entire structure, but for higher frequencies, displacements appear in opposite phases (Fig. 25).

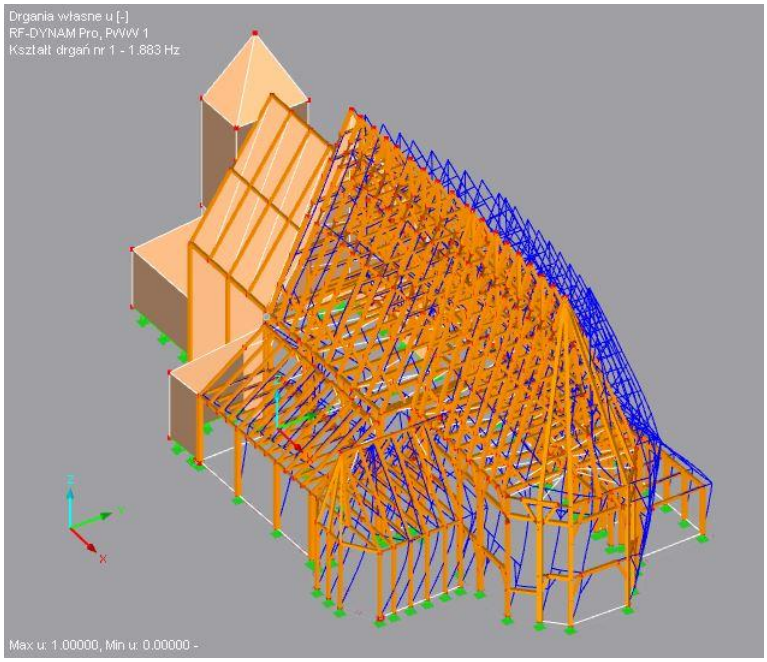

Fig. 24. Vibration mode related to the fundamental frequency f_1 = 1.883 Hz for the SE-S-0 model

In the model with stiffening panels (model SE-S-5), the calculated initial natural frequencies concerned the vibrations of only certain parts of the structure. These ware mainly lateral vibrations of the stiffening panels alone. Only the seventh calculated resonant frequency was related to the mode where the entire structure moved laterally (Fig. 26).

It is worth noting that in all the models, with and without stiffening panels, the frequencies that excite the whole body of the building (Table 7) are much higher than the

frequencies recorded during wind gusts in the actual structure (Fig. 13), which were described above in the "*Measurement of accelerations at a selected point*" section. It can be concluded that wind gusts are unable to induce dangerous resonant vibrations in the studied building.

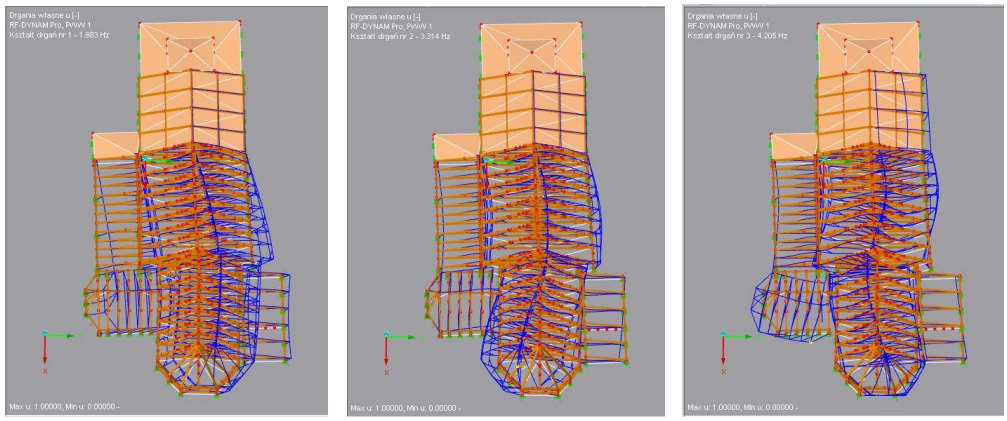

Fig. 25. Comparison of the first three modes of natural vibrations for the SE-S-0 model (f_1 = 1.883 Hz, f_2 = 3.314 Hz, f_3 = 4.205 Hz)

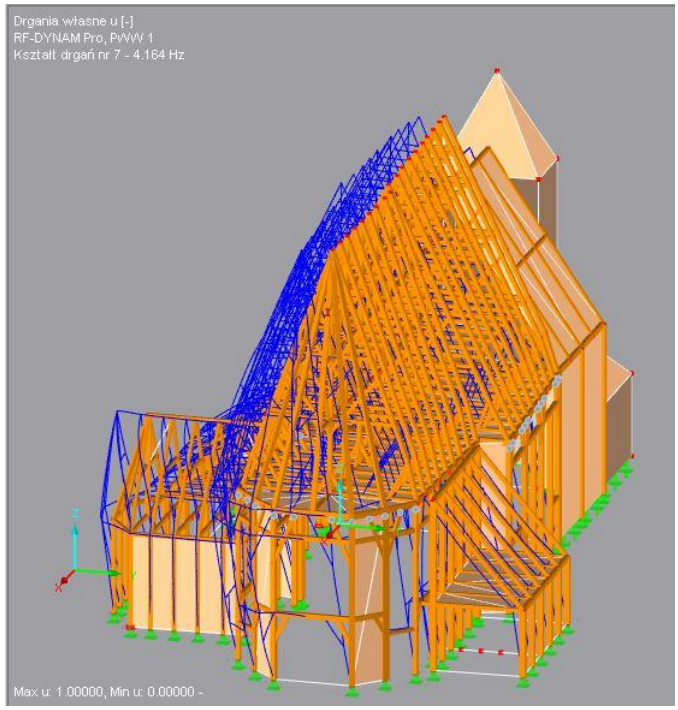

Fig. 26. Vibration mode related to the lowest natural frequency (f_7 = 4.164 Hz) for the SE-S-5 model, which excited the entire building body

Conclusions

The object of study was a historic wooden church located in Domachowo, Poland. The body of the building consists of several parts that differ in carpentry techniques and time of construction. The oldest part is built of log walls that are reinforced on the inside with a wooden frame structure. The complex spatial structure and historic character required an individual approach to the research programme. Observations have shown that the structure behaves elastically, i.e. significant deformation occurs only in strong wind gusts and the system returns to equilibrium as soon as the load ceases. For these reasons, it was decided to conduct continuous displacement monitoring at selected points to measure and record maximum displacements.

The inclinations of selected columns were measured continuously using inclinometers. The displacements at the top of the columns were determined based on the recorded values and assuming that the effect of the bending of the columns themselves is small. Simultaneously, the authors recorded atmospheric changes in the surroundings of the building, i.e. temperature and speed and direction of wind. The operation of the inclinometers was controlled and adjusted by means of monthly geodetic measurements. According to the performed measurements, it was concluded that there is a full correlation between the displacements of the columns and the wind action in the studied object.

Furthermore, the authors used an accelerometer to measure changes in acceleration during strong wind gusts at the top of the selected post. This study showed that the building's body is not excited by wind gusts. The main reason for this is the irregular action of gusts and the relatively low mass of the building compared to its rigidity. It was proved that the object's natural frequencies are higher than the frequency of pulses generated by wind gusts.

Based on the performed measurements and static and dynamic analyses, the authors concluded that the displacements caused by wind are within acceptable values. It was found that if the two short walls between the chancel and nave had more rigidity in the actual structure, the displacement values would have been much smaller. The actual technical condition of these walls is poor and the recorded displacement measurements are close to the results from the numerical model, where these stiffening panels were not taken into account in the calculations. Strengthening the elements of the walls situated at the connection of the nave and the chancel could considerably improve the rigidity of the structure, reducing its deformations and thus making it more resistant to dynamic loads.

The numerical model made it possible to analyze the effect of weaknesses in selected structural elements on the spatial work of the entire structure. The analysis demonstrated how reducing the cross-section of a wall element affects the extremes of stress and displacement. The authors also found that the spatial roof structure forms a rigid body and that the weakest elements are the posts in the nave and channel. The modal analyses in the calculation models revealed that wind gusts cannot induce resonance of the structure due to the considerable difference between the system's natural frequency and the frequencies generated by the wind.

The paper shows that the proposed author's method of geodetic static measurements supplemented by dynamic measurements using inclinometers is a very good tool for studying complex structures of historic buildings. Measurements of the structure’s dynamic response have proven to be a good tool for complementing geodetic measurements in creating and validating a numerical model of a complex spatial structure. They also provide a very good analytical tool for evaluating the actual operating conditions of the structure and for developing guidelines for practical conservation work.

Acknowledgments

This research was funded by the Rector of Poznan University of Technology, grant number: 0112/SIGR/0193. This support is gratefully acknowledged.

References

[1] J. Sola-Caraballo, J.M. Rincón-Calderón, C. Rivera-Gómez, J.A. López-Martínez, C. Galán-Marín, *On-Site Risk Assessment Methodology of Historic Timber Structures: The Case Study of Santa Cruz Church*, **Buildings**, **12**(7), 2022, Article Number: 935. DOI: 10.3390/buildings12070935.

[2] G. Barozzi, N. Cosentino, L. Lanzoni, A.M. Tarantino, *Safety assessment of historic timber structural elements*, **Case Studies in Construction Materials**, **8**, 2018, pp. 530-541. DOI: 10.1016/j.cscm.2018.04.006.

[3] K. Ericsson, E. Karawajczyk, R. Kliger, T. Lechner, E. Lukaszewska, W. Misztal, T. Nowak, *Non-destructive Testing of The Historic Timber Roof Structures of The National Museum in Stockholm, Sweden*. **International Journal of Heritage Architecture: Studies, Repairs and Maintence**. **2**. 2018, pp. 218-2229. DOI:10.2495/HA-V2-N2-218-229.

[4] A. Serafini, C. Gonzàlez-Longo, *Seventeenth and eighteenth century timber roof structures in Scotland:design, pathologies and conservation*, **Structural Analysis of Historical Constructions: Anamnesis, Diagnosis, Therapy, Controls**, Proceedings of the 10th International Conference on Structural Analysis of Historical Constructions (Editors: K. Van Balen and E. Verstrynge), CRC Press, 2016. DOI: 10.1201/9781315616995.

[5] H. Cruz, D. Yeomans, E. Tsakanika, N. Macchioni, A. Jorissen, M. Touza, M. Mannucci and P. B. Lourenço, *Guidelines for the on-site assessment of historic timber structures*. **International Journal of Architectural Heritage: Conservation, Analysis, and Restoration**, **9 (3)**, 2014, pp. 277-289. DOI: 10.1080/15583058.2013.774070.

[6] L. Reinprecht, **Diagnosis, Sterilization and Restoration of Damaged Timber Structures**, Faculty of Wood Sciences and technology, Technical University in Zvolen, Zvolen, 2016.

[7] N. Macchioni, A. Feio, U. Ruisinger, J. Machado, E. Tsakanika, D. Yeomans, *The Pren 17121: Historic Timber Structures - Guidelines for the On-Site Assessment of Load-Bearing Timber Structures*, **5 th International Conference on Structural Health Assessment of Timber Structures**, 2021.

[8] A. Cavalli, D. Cibecchini, M. Togni, H. S. Sousa, *A review on the mechanical properties of aged wood and salvaged timber*, **Construction and Building Materials**, **114**, 2016, pp. 681-687. DOI: 10.1016/j.conbuildmat.2016.04.001.

[9] M. Kloiber, M. Drdácký, J. S. Machado, M. Piazza, N. Yamaguchi, *Prediction of mechanical properties by means of semi-destructive methods: A review*, **Construction and Building Materials**, **101**(2), 2015, pp. 1215-1234. DOI: 10.1016/j.conbuildmat.2015.05.134.

[10] T. Nowak, F. Patalas, A. Karolak, *Estimating Mechanical Properties of Wood in Existing Structures—Selected Aspects*, **Materials**, **14**, 2021, Article Number: 1941. DOI:10.3390/ma14081941.

[11] F. Arriaga, C. Osuna-Sequera, I. Bobadilla, M. Esteban, *Prediction of the mechanical properties of timber members in existing structures using the dynamic modulus of elasticity and visual grading parameters*, **Construction and Building Materials**, **322**, 2022, Article Number: 126512. DOI: 10.1016/j.conbuildmat.2022.126512.

[12] V. Nasir, S. Ayanleye, S. Kazemirad, F. Sassani, S. Adamopoulos, *Acoustic emission monitoring of wood materials and timber structures: A critical review*, **Construction and Building Materials**, **350**, 2022, Article Number: 128877, DOI: 10.1016/j.conbuildmat.2022.128877.

[13] J. Jaskowska-Lemańska, E. Przesmycka, *Semi-Destructive and Non-Destructive Tests of Timber Structure of Various Moisture Contents*, **Materials**, **14**, 2021, Article Number: 96. DOI: 10.3390/ma14010096.

[14] A. Cavalli, M. Togni, *Monitoring of historical timber structures: state of the art and prospective*, **Journal of Civil Structural Health Monitoring**, **5**, 2015, pp. 107–113, DOI: 10.1007/s13349-014-0081-8.

[15] L.J. Prendergast, K. Gavin, *A review of bridge scour monitoring techniques*, **Journal of Rock Mechanics and Geotechnical Engineering**, **6** (2), 2014, pp.138–149. DOI: 10.1016/j.jrmge.2014.01.007.

[16] P.F. Giordano, L.J. Prendergast, M.P. Limongelli, *The Value of Different Monitoring Systems in the Management of Scoured Bridges*, **Experimental Vibration Analysis for Civil Engineering Structures. Lecture Notes in Civil Engineering**, (Editors: Z. Wu, T. Nagayama, J. Dang and R. Astroza), Vol. 224, Springer Cham, 2023. DOI: 10.1007/978-3-030-93236-7_11.

[17] Ch. Xue, P. Psimoulis, A. Horsfall, Q. Zhang, X. Meng, *Assessment of the accuracy of low-cost multi-GNSS receivers in monitoring dynamic response of structures*, **Applied Geomatics**, **15**(2), 2022. pp: 315-326, Special Issue: SI. DOI: 10.1007/s12518-022-00482-8.

[18] Y. Deng, Y. Li, A. Li, *Seismic safety assessments of historical timber buildings using updated finite element models: Case study of Yingxian wooden pagoda, China*, **Journal of Building Engineering**, **63**, Part A, 2023, Article Number: 105454. DOI: 10.1016/j.jobe.2022.105454.

[19] C. Miedziałowski, J. Malesza, M. Szkobodziński, *Structural interaction of tower with walls and flying buttress system in historic church*, **Wiadomości Konserwatorskie**, **45**, 2016, pp. 76-86. DOI: 10.17425/WK45BUTTRES.

[20] A. Różański, T. Jurek, P. Marciniak, P. Łobodzińska, U. Schaaf, *Interdisciplinary Research on Wooden Architecture in Poland. A Case Study of the Wooden Church in Domachowo*, **Archaeologia Historica Polona**, **28**, 2020, pp. 175–197. DOI: 10.12775/AHP.2020.007.

[21] S. Logothetis, A. Delinasiou, E. Stylianidis, *Building Information Modelling for Cultural Heritage: A review*. **ISPRS Annals of Photogrammetry, Remote Sensing and Spatial Information Sciences**, **II-5/W3**, 2015, pp. 177-183. DOI: 10.5194/isprsannals-II-5-W3-177-2015

[22] F. Diara, *HBIM Open Source: A Review*, **International Journal of Geo-Information**, **11**(9), 2022, Article Number: 472. DOI: 10.3390/ijgi11090472.

[23] C. Bianchini, G. Potestà, *BIM for built cultural heritage: the case of the Baptistery of San Giovanni in Florence*, **IOP Conference Series: Materials Science and Engineering**, **949**, 2020, Article Number: 012044. DOI: 10.1088/1757-899X/949/1/012044.

[24] Z.M. Pawlak, I. Wyczałek, P. Marciniak, *Two Complementary Approaches toward Geodetic Monitoring of a Historic Wooden Church to Inspect Its Static and Dynamic Behavior*, **Sensors**, **23**, 2023, Article Number: 8392. DOI: 10.3390/s23208392.

[25] P. Marciniak, Z. Pawlak, I. Wyczałek, *The Dynamic-Static Method (DSM) for Structural Displacement Analysis Using the Example of a Wooden Church in Domachowo (Poland)*, **International Archives of the Photogrammetry, Remote Sensing and Spatial Information Sciences - ISPRS Archives,** 2023, XLVIII-M-2-2023, pp. 1001–1006. DOI:10.5194/isprs-archives-XLVIII-M-2-2023-1001-2023.

Received: October 30, 2023
Accepted: August 10, 2024